Journal of Power Sources 185 (2008) 1107–1114

Contents lists available at ScienceDirect

Journal of Power Sources

journal homepage: www.elsevier.com/locate/jpowsour

Energy and exergy analyses of a hybrid molten carbonate fuel cell system

R. Rashidi [a], I. Dincer [a,*], P. Berg [b]

[a] Faculty of Engineering and Applied Science, University of Ontario Institute of Technology, 2000 Simcoe Street North, Oshawa, Ontario, Canada L1H 7K4
[b] Faculty of Science, University of Ontario Institute of Technology, 2000 Simcoe Street North, Oshawa, Ontario, Canada L1H 7K4

ARTICLE INFO

Article history:
Received 25 May 2008
Received in revised form 19 July 2008
Accepted 21 July 2008
Available online 30 July 2008

Keywords:
Energy
Exergy
Efficiency
Molten carbonate fuel cell
Performance
Power

ABSTRACT

This study deals with the energy and exergy analysis of a molten carbonate fuel cell hybrid system to determine the efficiencies, irreversibilities and performance of the system. The analysis includes the operation of each component of the system by mass, energy and exergy balance equations. A parametric study is performed to examine the effect of varying operating pressure, temperature and current density on the performance of the system. Furthermore, thermodynamic irreversibilities in each component of the system are determined. An overall energy efficiency of 57.4%, exergy efficiency of 56.2%, bottoming cycle energy efficiency of 24.7% and stack energy efficiency of 43.4% are achieved. The results demonstrate that increasing the stack pressure decreases the overpotential losses and, therefore, increases the stack efficiency. However, this increase is limited by the remaining operating conditions and the material selection of the stack. The fuel cell and the other components in which chemical reactions occur, show the highest exergy destruction in this system. The compressor and turbine on the other hand, have the lowest entropy generation and, thus, the lowest exergy destruction.

1. Introduction

With substantial investments by both the private and public sectors, fuel cell technology is rapidly advancing. Due to the high-energy efficiency and clean environmental performance, fuel cells are regarded as a potential reliable future source of energy supply. However, the large initial capital costs of fuel cell technology have offset the advantages they offer and slowed down their adoption for widespread use. The main reasons for using fuel cells in power generation can be characterized as the need for pollution reduction, back-up power, diversification of energy supply and, hence, a reduction of foreign energy dependency (e.g., [1]).

Construction of the first molten carbonate fuel cell (MCFC) dates back to 1960 by Broers and Ketelaar [2]. They reported a high temperature fuel cell that employed an electrolyte comprising a mixture of alkali metal carbonates constrained within a disc of magnesium oxide, operating for 6 months. The operating temperature was well above the melting point of the carbonates and, therefore, the charge transport within the molten electrolyte was facilitated by means of carbonate ions (CO_3^{2-}). Although there have been many changes in the materials used for construction of this type of fuel cell over the last 40 years, the operating principle remains the same.

The present demonstration and research projects of MCFC stacks and systems show a wide range of power output. Power ranges from a few kilowatts to several megawatts are achievable. Hospitals, hotels, office buildings and industrial applications could be the place of choice to test these projects.

Despite numerous research on MCFC systems, there are still many opportunities for further improvements of this technology. Enhancing the component durability to achieve the goal of a 40,000 h lifetime, increasing the cell performance and reducing costs in order to make the systems economically viable in the power producing market are the main targets in competitive improvements. One way of achieving the highest efficiency possible from MCFC systems is to recover residual pressure and waste heat via gas turbine bottoming cycle and cogeneration [3].

Maru et al. [4] investigated the performance of a 20 MW internal reforming MCFC-based power plant fuelled with natural gas. They predicted an efficiency of 75% when a gas turbine was coupled with the fuel cell via heat exchangers. In another study, Liese and Gemmen [5] predicted the performance of an almost identical 1 MW internal reforming MCFC-based power plant fuelled with natural gas working under ambient pressure condition. Again, the gas turbine was coupled with the fuel cell via heat exchangers and the expected efficiency of the system was reported to be 75%. Moreover, Gnann [6] conducted a similar study to predict the performance of

* Corresponding author. Tel.: +1 905 721 8668x2573; fax: +1 905 721 3370.
E-mail addresses: ramin.rashidi@mycampus.uoit.ca (R. Rashidi), ibrahim.dincer@uoit.ca (I. Dincer), peter.berg@uoit.ca (P. Berg).

0378-7753/$ – see front matter © 2008 Elsevier B.V. All rights reserved.
doi:10.1016/j.jpowsour.2008.07.061

Nomenclature

AN	anode
b	cell active surface area width (m)
CA	cathode
dx	differential length of the cell (m)
E	voltage (V)
E^0	Nernst potential (V)
F	Faraday constant (C mol^{-1})
$\Delta\bar{g}_f$	molar Gibbs free energy of formation (kJ mol^{-1})
$\bar{h}$	molar absolute enthalpy (kJ kmol^{-1})
in	inlet
I	current (A)
L	total length of the cell (m)
LHV	fuel lower heating value (kJ kg^{-1})
m	mass flow rate (kg s^{-1})
n	molar flow rate (mol s^{-1})
out	outlet
P	pressure (atm)
Q	heat (W)
R	universal gas constant (8.3145 J mol^{-1} K^{-1})
$\bar{s}$	molar entropy (kJ kmol^{-1} K^{-1})
T	temperature (K)
U	utilization factor
$\dot{W}$	power (W)
X	mole fraction
z	number of electrons transferred for each molecule of fuel (z = 4)

Greek letters

α	heat transfer coefficient (W K^{-1} m^{-2})
η	impedance related to electrode overpotential (Ω m^2)
$\bar{\Psi}$	molar exergy (kJ kmol^{-1})
$\bar{\Psi}^{chemical}$	molar chemical exergy (kJ kmol^{-1})

Subscripts

a	anode
act	activation
conc	concentration
c	cathode
C	compressor
CB	catalytic burner
Dest	destruction
FC	fuel cell
HE	heat exchanger
MC	mixing chamber
ohm	ohmic
RHE	regenerative heat exchanger
tot	total
T	turbine
0	standard reference state (P = 1 atm, T_0 = 298.15 K)

a 250 kW range MCFC-based power plant under ambient pressure condition. This system was not coupled with a gas turbine and the efficiency of the system was reported to be about 47%. In the studies of De Simon et al. [3] on a molten carbonate fuel cell hybrid system, a stack maximum efficiency of 60.3%, global process electrical efficiency of 51.1% and co-generative efficiency of 74%, based on their base case, is achieved.

According to their study and performing a sensitivity analysis, there is still room for improvement in electrical efficiency by increasing steam to methane ratio and pressure, and decreasing air feed rate. Therefore, the combination of fuel cell and power plant as the bottoming cycle could produce better performances and higher efficiencies in general and further research in this field is required.

To the best knowledge of the authors, no studies have been undertaken to investigate the performance of this MCFC hybrid system through exergy analysis. In this paper, energy and exergy analysis of the fuel cell stack and the overall combined system are performed. Moreover, system efficiency and irreversibilities in different compartments of the system are obtained. A parametric study to investigate the effect of operating conditions on the efficiencies and irreversibilities found previously was also undertaken.

2. System description

A typical molten carbonate fuel cell stack running on natural gas may be operated with an efficiency of about 50%. However, when the MCFC is combined with the catalytic burner, reformer and the turbine, higher efficiencies are expected. Natural gas after filtration and desulphurization is mixed with steam which is preheated from the stack exhaust gases. The mixture is then heated further in a regenerative heat exchanger and fed to the reformer. After the reforming reaction takes place, the exit gas is passed through the regenerative heat exchanger again and finally fed to the anode of the MCFC. A fraction of hydrogen input, and also some residual CH_4, pass the anode unreacted. Therefore, following the electrochemical reaction in the stack, the exhaust mixed with a fraction of cathode exhaust is burnt in the catalytic burner in order to produce the heat necessary for the endothermic reactions taking place in the reformer. The heat produced in the catalytic burner is directly transferred to the reformer and it is assumed that there is no heat transfer with the surroundings in this study. The catalytic burner exhaust, which is a hot mixture rich in CO_2, is mixed with fresh air coming from the compressor and fed to the cathode. Thus, Fig. 1 shows a schematic of the system for this study. The system studied here is the modified version of the one studied by De Simon et al. [3].

In the following analysis section, the MCFC stack is treated as one unit, without resolution of the cell level dynamics, and the whole power generation system in divided into different compartments, like compressor, pumps, etc. Starting with mass, energy and exergy balances for each component and the whole system, the exergy losses and overall efficiencies of the hybrid system are found.

3. Thermodynamic analysis

Similar to all other types of fuel cells, the operating principle of MCFCs is basically the indirect combination of hydrogen and oxygen to produce water, employing an electrolyte, thereby producing electrical energy and heat. Fig. 2 shows the basic characteristics of a molten carbonate fuel cell (MCFC) and the anode and cathode half-cell reactions that take place. The assumptions made in this analysis are as follows:

- Steady state operation for all components.
- All units are based on SI unit system; with e.g., kPa for pressure, K for temperature and kJ kg^{-1} for enthalpy.
- All stream gases are ideal gases and, therefore, ideal gas properties using EES (Engineering Equation Solver) software are employed.
- Hydrogen utilization factor is taken to be 70% in this study.
- 85% of methane is reformed in the reformer and the rest is simply passing through the fuel cell without any chemical reaction but burnt completely in the catalytic burner.

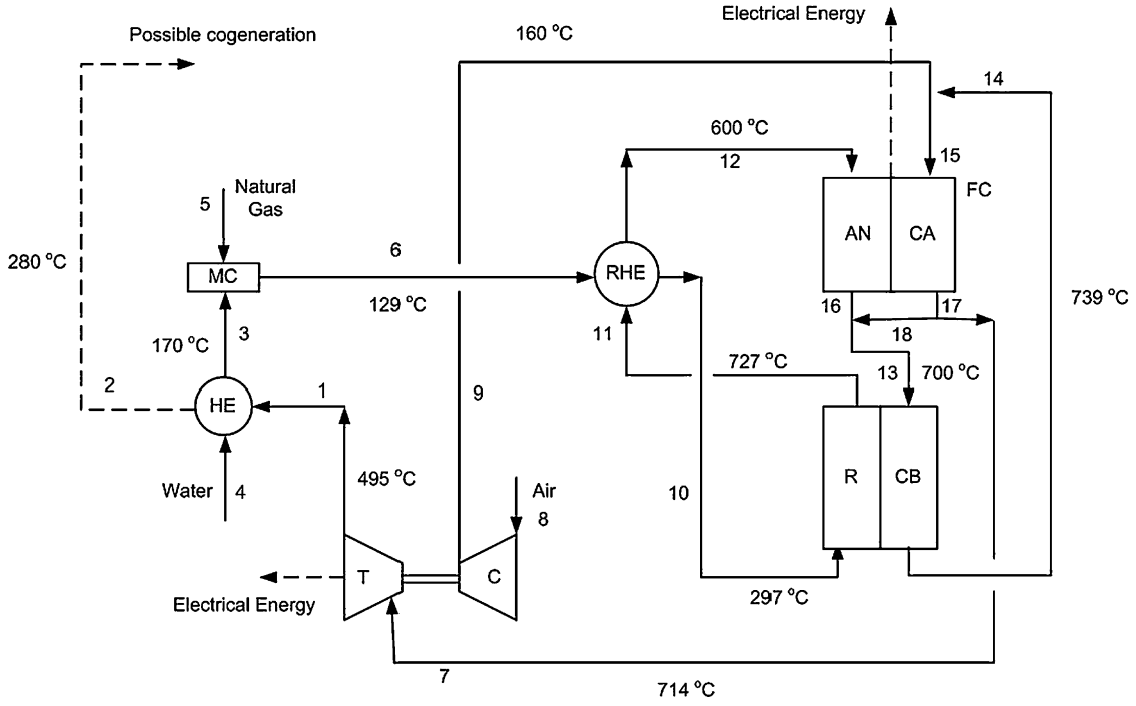

Fig. 1. Schematic of the system under consideration (HE: heat exchanger, RHE: regenerative heat exchanger, FC: fuel cell, MC: mixing chamber, CB: catalytic burner, R: reformer, T: turbine, C: compressor, CA: cathode, AN: anode).

- The heat exchanger, pumps, compressor and turbine are adiabatic and, hence, no heat transfer occurs between them and the surroundings.
- All kinetic and potential exergetic terms are negligible.
- The chemical exergetic term does not change in the turbine, pumps, compressor or the heat exchanger.
- The outlet of the cathode, after increasing the temperature of the inlet water, is discharged to the environment. (It is possible to use this high temperature mixture in a cogeneration system and achieve higher total efficiencies.)
- The ambient temperature and pressure are constant (T_0 and P_0) and would obviously change the system exergetic efficiency if they are subjected to any change.
- The total heat required for the reforming reactions in the reformer (the reforming reaction is endothermic) is supplied from the catalytic burner and no heat is lost from these systems.
- Some fraction of heat generated by the stack is lost due to convective cooling and radiation, the rest exits with the cathode exhaust.

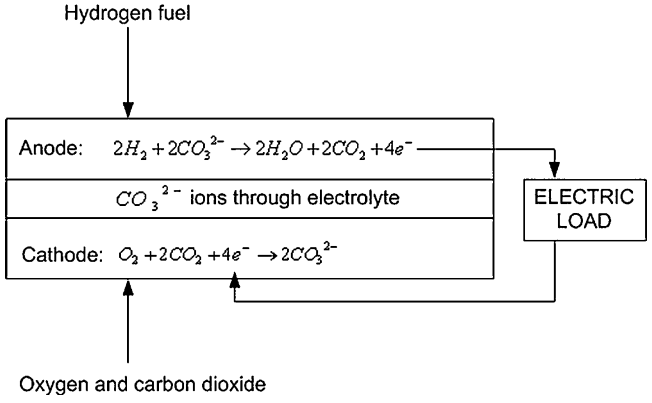

Fig. 2. Operating principle of the molten carbonate fuel cell.

- The combination of a compressor and turbine as a turbocharger is used in this system. Therefore, a fraction of power produced by the turbine is used in the compressor and the rest is a useful power output.
- The compressor increases the inlet air pressure from 1 to 4 atm.
- Molar flow rates for streams where any chemical reaction takes place can be used in order to find the energy balance equations.
- Air is an ideal gas with a composition of 21% oxygen and 79% nitrogen.
- Metal dusting reactions which result in a deteriorating performance of the MCFC, are neglected.
- Isentropic operation is assumed for the compressor and the turbine.
- The inlet mass flow rate of natural gas, water and air are taken from De Simon et al. [3] which are 74.5, 252 and 2250 kg h^{-1} respectively.

3.1. Half-cell reactions

Hydrogen reacts with carbonate ions at the anode to produce water, carbon dioxide and electrons which are transferred to the cathode through the external circuit. The water–gas shift reaction is another reaction that can occur at the anode in the presence of CO.

Anode:

$$2H_2 + 2CO_3^{2-} \rightarrow 2H_2O + 2CO_2 + 4e^-$$

$$CO + H_2O \rightarrow CO_2 + H_2 \quad \text{(water–gas shift reaction)}$$

The cathode reaction reads:

$$O_2 + 2CO_2 + 4e^- \rightarrow 2CO_3^{2-},$$

Resulting in the overall reaction:

$$\frac{1}{2}O_2 + H_2 \rightarrow H_2O$$

The carbonate ions migrate through the electrolyte from cathode to anode. In contrast to the PEM fuel cell and alkaline fuel cell, CO_2 is a major component in the cathode reaction. Oxygen supplied pure or with air from the environment reacts with the CO_2 produced at the anode to yield carbonate ions. CO_2 can be transferred to the cathode input via two methods: Using an external recirculation of the anode exhaust after a complete combustion process or simply using a CO_2 permeable membrane.

On the anode side, hydrogen is generated from a natural gas steam reforming process. It could also be provided directly from the hydrogen produced by electrolysis of water or other methods. Using a catalyst (usually nickel), methane, the main energy carrier in natural gas, reacts with water to produce the hydrogen needed for the anode use. Since this process is endothermic, the waste heat from the fuel cell is used in this reaction and, therefore, an overall improvement in the total efficiency can be achieved. The reaction that takes place in the steam reforming of methane is as follows:

$$CH_4 + H_2O \rightarrow CO + 3H_2 \qquad \text{(steam reforming of methane)}$$

However, since the water–gas shift reaction is also taking place in the reformer, the exit gas consists of a composition of CO, CO_2 and H_2O.

We now move on to the thermodynamic analysis and write the mass, energy and exergy balance equations for different compartments of the system as follows (see Fig. 1):

3.2. Heat exchanger (HE)

Water input at (4) is heated to 170 °C through the heat exchanger. The burner exhaust after exchanging heat with water can be used for cogeneration purposes.

The mass balance equation for the turbine exhaust passing through the HE is

$$\sum_i \dot{n}_{i,1} = \sum_i \dot{n}_{i,2} \tag{1a}$$

$$\dot{m}_1 = \dot{m}_2 \tag{1b}$$

where 'i' is the species entering and leaving the heat exchanger, 'n' and '$\dot{m}$' denote molar and mass flow rates, respectively.

No reaction takes place in this heat exchanger. Therefore, the water composition leaves the heat exchanger unchanged and the mass flow rate remains the same.

$$\dot{n}_3 = \dot{n}_4 \tag{1c}$$

$$\dot{m}_3 = \dot{m}_4 \tag{1d}$$

The energy balance equation is

$$\dot{n}_3\bar{h}_3 + \sum_{i=1}^{N} \dot{n}_{i,2}\bar{h}_{i,2} = \dot{n}_4\bar{h}_4 + \sum_{i=1}^{N} \dot{n}_{i,1}\bar{h}_{i,1} \tag{1e}$$

where $\bar{h}_i$ is the molar enthalpy.

The exergy balance equation reads

$$\dot{n}_4\bar{\Psi}_4 + \sum_{i=1}^{N} \dot{n}_{i,1}\bar{\Psi}_{i,1} - \dot{n}_3\bar{\Psi}_3 - \sum_{i=1}^{N} \dot{n}_{i,2}\bar{\Psi}_{i,2} - \mathrm{Ex}_{\mathrm{dest,HE}} = 0 \tag{1f}$$

where $\mathrm{Ex}_{\mathrm{dest,HE}}$ is the exergy destruction; $\bar{\Psi}_i$ is the molar flow exergy (i.e., availability).

3.3. Mixing chamber (MC)

Natural gas (5) and water (3) are mixed together in the mixing chamber and the output (6) is directed towards the regenerative heat exchanger.

The mass balance equation is

$$\dot{m}_3 + \dot{m}_5 = \dot{m}_6 \tag{2a}$$

The energy balance equation is

$$\dot{n}_3\bar{h}_3 + \dot{n}_5\bar{h}_5 = \dot{n}_6\bar{h}_6 \tag{2b}$$

The exergy balance equation is

$$\dot{n}_3\bar{\Psi}_3 + \dot{n}_5\bar{\Psi}_5 - \dot{n}_6\bar{\Psi}_6 - \mathrm{Ex}_{\mathrm{dest,MC}} = 0 \tag{2c}$$

3.4. Turbine (T)

Hot depleted cathode gas (7) enters the turbine and leaves at (1) to produce power necessary to run the compressor as well as to produce electrical power output.

The mass balance equations are

$$\sum_i \dot{n}_{i,1} = \sum_i \dot{n}_{i,7} \tag{3a}$$

$$\dot{m}_1 = \dot{m}_7 \tag{3b}$$

The energy balance equation reads

$$\sum_{i=1}^{N} \dot{n}_{i,7}\bar{h}_{i,7} - \sum_{i=1}^{N} \dot{n}_{i,1}\bar{h}_{i,1} - \dot{W}_{\mathrm{s,net}} = 0 \tag{3c}$$

where $\dot{W}_{\mathrm{s,net}}$ is the net electrical power output from the turbine. A fraction of total power produced in the turbine is used in the compressor to compress air.

The exergy balance equation becomes

$$\sum_{i=1}^{N} \dot{n}_{i,7}\bar{\Psi}_{i,7} - \sum_{i=1}^{N} \dot{n}_{i,1}\bar{\Psi}_{i,1} - \dot{W}_{\mathrm{s,net}} - \mathrm{Ex}_{\mathrm{dest,T}} = 0 \tag{3d}$$

3.5. Compressor (C)

Air from the environment (8) enters the compressor and high pressure air leaves at (9). Power to run the compressor is supplied by the turbine.

The mass balance equation is

$$\dot{n}_8 = \dot{n}_9 \tag{4a}$$

$$\dot{m}_8 = \dot{m}_9 \tag{4b}$$

The energy balance equation takes the form

$$\dot{n}_8\bar{h}_8 - \dot{n}_9\bar{h}_9 + \dot{W}_{\mathrm{x}} = 0 \tag{4c}$$

where $\dot{W}_{\mathrm{x}}$ is the fraction of turbine electrical energy used in the compressor to compress the inlet air.

The exergy balance equation reads

$$\dot{n}_8\bar{\Psi}_8 - \dot{n}_9\bar{\Psi}_9 + \dot{W}_{\mathrm{x}} - \mathrm{Ex}_{\mathrm{dest,C}} = 0 \tag{4d}$$

3.6. Regenerative heat exchanger (RHE)

The mixture of methane and water (6) is passed through the regenerative heat exchanger and leaves at (10). It is heated by the excess heat from the reformer stream (11–12).

The mass balance equations are

$$\sum_i \dot{n}_{i,6} = \sum_i \dot{n}_{i,10} \tag{5a}$$

$$\sum_i \dot{n}_{i,11} = \sum_i \dot{n}_{i,12} \tag{5b}$$

$$\dot{m}_6 = \dot{m}_{10} \tag{5c}$$

$$\dot{m}_{11} = \dot{m}_{12} \tag{5d}$$

The energy balance equation reads

$$\sum_{i=1}^{N} \dot{n}_{i,6}\bar{h}_{i,6} + \sum_{i=1}^{N} \dot{n}_{i,11}\bar{h}_{i,11} - \sum_{i=1}^{N} \dot{n}_{i,10}\bar{h}_{i,10} - \sum_{i=1}^{N} \dot{n}_{i,12}\bar{h}_{i,12} = 0 \tag{5e}$$

The exergy balance equation is

$$\sum_{i=1}^{N} \dot{n}_{i,6}\bar{\Psi}_{i,6} + \sum_{i=1}^{N} \dot{n}_{i,11}\bar{\Psi}_{i,11} - \sum_{i=1}^{N} \dot{n}_{i,10}\bar{\Psi}_{i,10} - \sum_{i=1}^{N} \dot{n}_{i,12}\bar{\Psi}_{i,12} - \mathrm{Ex}_{\mathrm{dest,RHE}} = 0 \tag{5f}$$

3.7. Reformer (R)

The mixture of methane and water (10) enters the reformer and after the methane reforming reaction occurs, it leaves at (11).

The mass balance equations are

$$\sum_{i} \dot{n}_{i,10} = \sum_{i} \dot{n}_{i,11} \tag{6a}$$

$$\dot{m}_{10} = \dot{m}_{11} \tag{6b}$$

The energy balance equation reads

$$-\sum_{i=1}^{N} \dot{n}_{i,11}\bar{h}_{i,11} + \sum_{i=1}^{N} \dot{n}_{i,10}\bar{h}_{i,10} + \dot{Q}_{\mathrm{R}} = 0 \tag{6c}$$

where $\dot{Q}_{\mathrm{R}}$ is the heat transferred from the catalytic burner (CB) for the endothermic reaction taking place inside the reformer.

The exergy balance equation is given by

$$-\sum_{i=1}^{N} \dot{n}_{i,11}\bar{\Psi}_{i,11} + \sum_{i=1}^{N} \dot{n}_{i,10}\bar{\Psi}_{i,10} - (1 - \frac{T_0}{T_{\mathrm{RF}}})\dot{Q}_{\mathrm{R}} - \mathrm{Ex}_{\mathrm{dest,RHE}} = 0 \tag{6d}$$

where T_{RF} is the average reformer body temperature.

3.8. Catalytic burner (CB)

The exit gas mixture from the MCFC (13) enters the catalytic burner and in order to produce CO_2 for the cathode (14), it is burnt with excess O_2.

The mass balance equations are

$$\sum_{i} \dot{n}_{i,13} = \sum_{i} \dot{n}_{i,14} \tag{7a}$$

$$\dot{m}_{13} = \dot{m}_{14} \tag{7b}$$

The energy balance equation reads

$$-\sum_{i=1}^{N} \dot{n}_{i,14}\bar{h}_{i,14} + \sum_{i=1}^{N} \dot{n}_{i,13}\bar{h}_{i,13} - \dot{Q}_{\mathrm{CB}} = 0 \tag{7c}$$

The exergy balance equation is given by

$$-\sum_{i=1}^{N} \dot{n}_{i,14}\bar{\Psi}_{i,14} + \sum_{i=1}^{N} \dot{n}_{i,13}\bar{\Psi}_{i,13} - (1 - \frac{T_0}{T_{\mathrm{CB}}})\dot{Q}_{\mathrm{CB}} - \mathrm{Ex}_{\mathrm{dest,CB}} = 0 \tag{7d}$$

where $\dot{Q}_{\mathrm{CB}}$ is the heat lost from the catalytic burner which is provided to the reformer; T_{CB} is the average body temperature of the catalytic burner.

3.9. MCFC (FC)

The molten carbonate fuel cell is the main component of the combined system under consideration. Its main components are the anode, cathode and the electrolyte. However, we treat the MCFC as one unit, consisting of anode and cathode, without resolving the unit cell and stack level dynamics (see Eqs. (20)–(22) below).

The mass balance equations are

$$\sum_{i} \dot{n}_{i,12} = \sum_{i} \dot{n}_{i,16} \tag{8a}$$

$$\dot{m}_{12} = \dot{m}_{16} \tag{8b}$$

$$\sum_{i} \dot{n}_{i,15} = \sum_{i} \dot{n}_{i,17} \tag{8c}$$

$$\dot{m}_{15} = \dot{m}_{17} \tag{8d}$$

The energy balance equation reads

$$\sum_{i=1}^{N} \dot{n}_{i,15}\bar{h}_{i,15} - \sum_{i=1}^{N} \dot{n}_{i,17}\bar{h}_{i,17} + \sum_{i=1}^{N} \dot{n}_{i,12}\bar{h}_{i,12} - \sum_{i=1}^{N} \dot{n}_{i,16}\bar{h}_{i,16} - \dot{Q}_{\mathrm{FC}} - \dot{W}_{\mathrm{FC}} = 0 \tag{8e}$$

The exergy balance equation becomes

$$\sum_{i=1}^{N} \dot{n}_{i,15}\bar{\Psi}_{i,15} - \sum_{i=1}^{N} \dot{n}_{i,17}\bar{\Psi}_{i,17} + \sum_{i=1}^{N} \dot{n}_{i,12}\bar{\Psi}_{i,12} - \sum_{i=1}^{N} \dot{n}_{i,16}\bar{\Psi}_{i,16} - (1 - \frac{T_0}{T_{\mathrm{FC}}})r\dot{Q}_{\mathrm{FC}} - \dot{W}_{\mathrm{FC}} - \mathrm{Ex}_{\mathrm{dest,FC}} = 0 \tag{8f}$$

where T_{FC} is the average bulk temperature of the fuel cell; $\dot{W}_{\mathrm{FC}}$ is the electrical energy output from the MCFC; 'r' is the percentage of heat transferred through radiation or convection by the cell walls.

Current, current density and voltage calculation give

$$\text{Molar } O_2 \text{ usage} = \mathrm{I}/2F \tag{9a}$$

$$\text{Molar CO usage} = \mathrm{I}/2F \tag{9b}$$

$$\text{Stack power} = \text{cell voltage} \times i \times \text{active surface area} \times \text{number of cells} \tag{10}$$

where 'I' is the current in A ($i = I/A$).

The molar flow rates can simply be substituted by the ratio of mass flow rate and molar weight of that species.

The molar enthalpy and entropy can be found as follows (e.g., [7]):

$$\bar{h} = RT\left(\beta_1 + \frac{\beta_2}{2}T + \frac{\beta_3}{3}T^2 + \frac{\beta_4}{4}T^3 + \frac{\beta_5}{5}T^4 + \frac{\beta_6}{T}\right) \tag{11a}$$

$$\bar{s} = R(\beta_1 \ \ln(T) + \beta_2 T + \frac{\beta_3}{2}T^2 + \frac{\beta_4}{3}T^3 + \frac{\beta_5}{4}T^4 + \beta_7 \tag{11b}$$

where β_i is taken from JANAF tables [8].

The molar exergy term is the sum of physical, thermal and chemical exergetic terms as follows:

$$\bar{\Psi}_i = (\bar{h}_i(T) - \bar{h}_i(T_0)) - T_0(\bar{s}_i(T) - \bar{s}_i(T_0)) + RT_0 \ \ln(X_i) + \bar{\Psi}_i^{\mathrm{chemical}} \tag{12}$$

where X_i is the mole fraction of species 'i' and $\bar{\Psi}_i^{\mathrm{chemical}}$ is the chemical exergy. The chemical exergy values are taken from the exergoecology portal [9]

The heat loss from the fuel cell is the sum of heat loss from anode and cathode as

$$\dot{Q}_{FC} = \dot{Q}_{cathode} + \dot{Q}_{anode} = \alpha^{c} b \int_0^L (T_{MCFC}(x) - T_0)\ dx + \alpha^{a} b \int_0^L (T_{MCFC}(x) - T_0)\ dx \quad (13)$$

where 'α' is the heat transfer coefficient, 'b' is the width of the active surface area of the cell and 'dx' is the differential length of the cell.

The hydrogen, CO and oxidant utilization factors are defined as

$$U_{H_2} = \frac{\dot{n}_{H_{2,11}} - \dot{n}_{H_{2,16}}}{\dot{n}_{H_{2,11}}} \quad (14a)$$

$$U_{CO} = \frac{\dot{n}_{CO_{11}} - \dot{n}_{CO_{16}}}{\dot{n}_{CO_{11}}} \quad (14b)$$

$$U_{CO_2} = \frac{\dot{n}_{CO_{2,15}} - \dot{n}_{CO_{2,17}}}{\dot{n}_{CO_{2,15}}} \quad (14c)$$

Therefore, considering the water produced in the fuel cell we have

$$\dot{n}_{H_2O,16} = \dot{n}_{H_2O,11} + \dot{n}_{H_2,11} U_{H_2} \quad (15)$$

Nitrogen is an inert gas and passes the cathode without any reaction. Therefore, we have

$$\dot{n}_{N_2,15} = \dot{n}_{N_2,17} \quad (16)$$

Calculation of the overall energy and exergy efficiencies of the hybrid system follows:

$$\eta_{energy} = \frac{\dot{W}_{FC} + \dot{W}_s - \dot{W}_x}{\dot{n}_{fuel} \times LHV} \quad (17)$$

$$\eta_{exergy} = \frac{\dot{W}_{FC} + \dot{W}_s - \dot{W}_x}{\sum_i (\dot{n}_i \times ex_i)} = 1 - \frac{\sum Ex_{dest}}{\sum_i (\dot{n}_i \times ex_i)} \quad (18)$$

where 'i' denotes the fuel, air and water at inlet; $\sum Ex_{dest}$ is the total exergy destruction in the compressor, turbine, heat exchanger, mixing chamber, fuel cell, reformer and catalytic burner. Moreover, if the cathode exhaust after the water heating is released to the environment, it should be included as exergy destruction.

The power output of the fuel cell can be as approximated as follows (e.g., [10]):

$$\dot{W}_{FC} = Eb \int_0^L i(x)\ dx \quad (19)$$

where 'L' is the total length of a cell and 'E' is the voltage approximated by

$$E = E^0 - i \times (\eta_{act} + \eta_{conc} + \eta_{ohm}) \quad (20)$$

Here, 'E^0' is the reversible open circuit voltage, 'η_{act}', 'η_{conc}' and 'η_{ohm}' are the activation, concentration and ohmic impedances, respectively. The bipolar plates and electrodes are assumed to be perfect conductors and therefore all ohmic losses are given by the resistance of the electrolyte against the flow of carbonate ions.

The following equations are taken from Koh et al. [11] for the reversible open circuit voltage (E^0) and the total irreversible losses (η_{total}):

$$E^0 = \frac{-\Delta \bar{g}_f}{zF} + \left[\frac{RT_{FC}}{2F} \times \ln \frac{P_{H_2,a} P_{CO_2,c} P_{O_2,c}{}^{0.5}}{P_{CO_2,a} P_{H_2O}} \right] \quad (21)$$

$$\eta_{total} = \eta_{act} + \eta_{conc} + \eta_{ohm} = 2.27 \times 10^{-9} \times \exp\left(\frac{6435}{T_{FC}}\right) \times P_{H_2}{}^{-0.42} P_{CO_2}{}^{-0.17} P_{H_2O}{}^{-1.0} + 7.505 \times 10^{-10} \times \exp\left(\frac{9298}{T_{FC}}\right) \times P_{O_2}{}^{-0.43} P_{CO_2}{}^{-0.09} + 0.5 \times 10^{-4} \times \exp\left[3016 \times \left(\frac{1}{T_{FC}} - \frac{1}{923}\right)\right] \quad (22)$$

where 'F' is the Faraday constant; '$\Delta \bar{g}_f$' is the molar Gibbs free energy of formation, 'P_i' is the partial pressure of species 'i' at the inlet and 'z' is the number of electrons transferred for each molecule of fuel.

Eq. (22) simply rolls all complex dynamics of the MCFC unit cell and stack level into one effective expression, given by a fit to experimental data in the form of polarization curves.

4. Results and discussion

The analysis presented above is applied to the hybrid system with varying operating pressure, temperature and current density to study the performance of the system. From this study, maximum energy and exergy efficiencies of 57.4% and 56.2% are obtained, respectively. The efficiency of the bottoming cycle defined as $(power_{turbine} - power_{compressor})/(power_{fuel} - power_{stack})$ is calculated as 24.7%. The energy and exergy efficiencies of the fuel cell are found to be 43.4%, 42.5%, respectively.

The variation of fuel cell voltage and irreversible voltage with current density at an operating pressure of 4 atm is shown in Fig. 3. It can be observed from the figure that, with an increase in current density, the cell voltage decreases. Higher current densities increase the irreversibilities in the cell and results in lower voltages. Concentration losses are the main reasons for the low output voltages at high current densities.

Fig. 4 shows the variation of power output and overall energy and exergy efficiencies of the system with current density at 4 atm. From the figure it can be seen that both fuel cell power output and overall hybrid system efficiencies initially increase at lower current densities reaching their peaks and finally decrease. The maximum power output is obtained as 418.2 kW at the current density of 0.4667 A cm^{-2} for corresponding maximum energy and exergy efficiency of 57.4% and 56.2%, respectively. At lower current densities, the molar flow rate of fuel and the power required by the auxiliary devices are low and, therefore, the efficiency increases to its peak value. Thereafter, the parasitic load and molar consumption of fuel increases at higher current densities and hence the efficiency decreases. Moreover, energy efficiencies are higher than exergy effi-

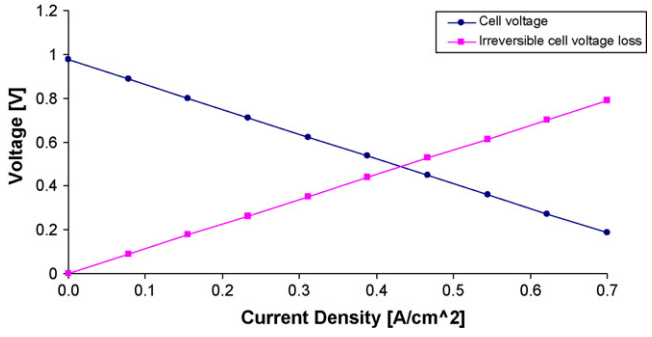

Fig. 3. Plot of operating voltage and irreversible cell voltage against the current density (at 4 atm).

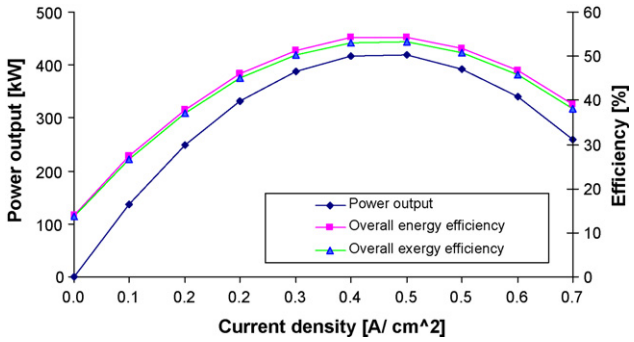

Fig. 4. Plot of stack power output and overall hybrid system energy and exergy efficiencies versus current density (at $P = 4$ atm).

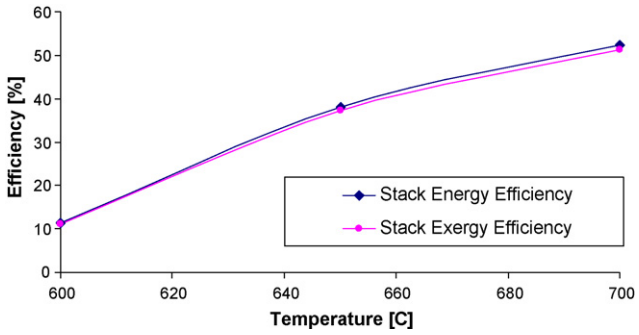

Fig. 6. Plot of stack energy and exergy efficiencies versus the variation in operating temperature (at 4 atm and current density of 0.5 A cm^{-2}).

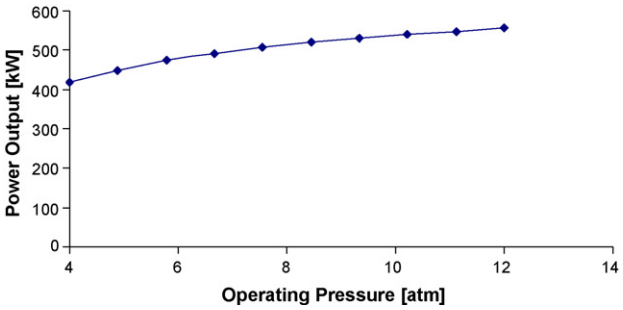

Fig. 7. Plot of the stack power output versus the operating pressure (at 650 °C and current density of 0.5 A cm^{-2}).

ciency which is due to the difference between energy and exergy content of the fuel.

Based on the exergy analysis, the fuel cell and the catalytic burner exhibit the maximum exergy destruction and, hence, any exergy improvements should be mainly focused on these compartments. Moreover, the heat exchanger shows a remarkable exergy loss because of a large temperature difference between the streams. The main exergy destructions are in the compartments where chemical reactions take place. Another main source of exergy destruction is from the exit of the heat exchanger. The exergy content of this stream with a fairly high temperature of 280 °C can be used for possible cogeneration purposes. Therefore, an additional 215 kW of power could be achieved if the exergy of this stream is used in a cogeneration system (e.g., [3]).

Fig. 5 summarizes the exergy destruction in different compartments of the hybrid system. Irreversibilities, and thus entropy generation, are the reasons for the exergy destruction. In order to improve the performance of the system is essential to minimize the exergy destructions which will result in increasing exergy efficiency. These exergy destructions are primarily affected by the operating conditions within the system and surrounding conditions.

Fig. 6 shows the energy and exergy efficiencies of the fuel cell at different operating temperatures. The operating pressure and current density were set at 4 atm and 0.5 A cm^{-2}, respectively. It can be seen that both energy and exergy efficiencies of the MCFC increase with the increase of temperature. This is due to the decrease in irreversibilities of the fuel cell with the increase of temperature. However, increasing the operating temperature is limited by the fuel cell material selection and other operating conditions.

Figs. 7 and 8 exhibit the power output, energy and exergy efficiencies of the fuel cell at different operating pressures. The operating temperature was 650 °C and the current density was set at 0.5 A cm^{-2}. The power output, and energy and exergy efficiencies of the MCFC increase with pressure. This is due to the decrease in irreversible losses, especially anode and cathode overpotentials. Although high pressure operation enhances the performance of the fuel cell, it requires a more powerful compressor, results in a bulky balance of plant and meets limitations to the stack sealing. There disadvantages of operating at high pressures can be so severe that a low pressure operation is often preferable.

Another approach in improving the overall performance of the combined system is through improving the bottoming cycle efficiency. Table 1 lists the overall energy and exergy efficiency improvements by an enhancement in the bottoming cycle efficiency.

Overall system efficiency can also be improved by using the exergy content of stream 2 as shown in Fig. 1. The flow exergy contained in this stream can be used as an input exergy into the fuel cell to maintain its operating temperature or can be used for any external co-generation purposes to produce more power output. According to this study, global exergetic efficiency can be increased by 15% when the 150 kW exergy wasted at point 2 is used in a

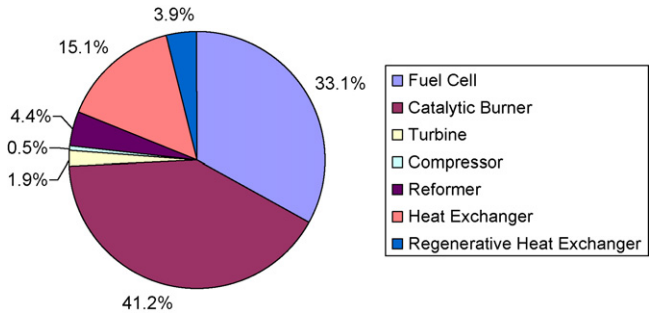

Fig. 5. Exergy destruction in different compartments of the hybrid system.

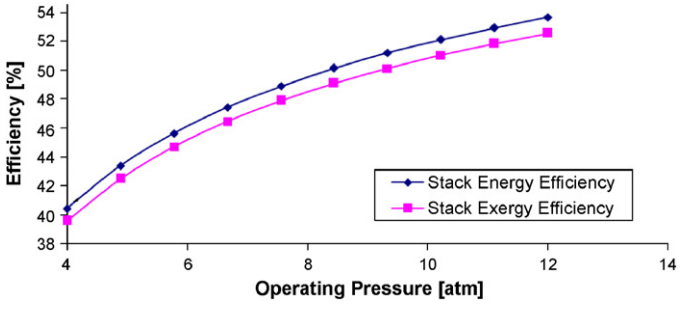

Fig. 8. Plot of the stack energy and exergy efficiency versus the operating pressure (at 650 °C and current density of 0.5 A cm^{-2}).

Table 1
Variation of overall energy and exergy efficiencies by varying the bottoming cycle energy efficiency

Bottoming cycle energy efficiency (%)	Overall energy efficiency (%)	Overall exergy efficiency (%)
6.4	51.7	50.6
7.2	52.1	51.1
8.1	52.6	51.5
8.0	53.0	51.9
9.7	53.4	52.3
10.5	53.9	52.7
11.4	54.3	53.2
12.2	54.7	53.6
13.0	55.1	53.9
13.9	55.6	54.4

co-generation power production. Similarly, a maximum energetic efficiency of 75% for the global system could be achieved upon the usage of the energy loss at point 2.

Finally, considering the environmental impact and sustainable development, the system is environmentally benign with very low output emissions. The waste heat generated is assumed to be used efficiently and, therefore, the whole hybrid system helps to improve the sustainability. Increasing the system efficiency leads to even higher sustainability and less environmental impacts. Environmental impact is classified as order destruction, source degradation and waste exergy emissions [12].

It is important to highlight that the exergy or energy content of a substance is a measure of its availability or usefulness to cause change and interact with respect to its surrounding environment [13,14]. Therefore, a thorough understanding of exergy analysis, exergetic efficiency and environmental impact of the hybrid systems leads to higher efficiencies and, consequently, improved performance.

5. Conclusions

An exergetic and energetic efficiency study of a hybrid MCFC system has been performed in this paper. In addition, a parametric study is undertaken to examine the effect of varying operating pressure, temperature and current density on the energy and exergy efficiencies of the fuel cell stack. It was found that, increasing the stack pressure and temperature decreases the overpotentials and, therefore, increases the stack efficiency. Although high operating pressures require an increase in the power input of the compressor, the net power produced by the system and the energy and exergy efficiencies increase with pressure. The fuel cell power output and overall hybrid system efficiency initially increase at lower current densities before peaking, then decrease with a further increase in current density. This suggests that there exists an optimal operating point in terms of current density with respect to system efficiency. The maximum power output was obtained as 418.2 kW at 0.4667 A cm^{-2}. It was also found that maximum global energy efficiency of 57.35% and exergy efficiency of 56.16% is achievable. The bottoming cycle exhibits an energy efficiency of 24.7%. The MCFC stack and the catalytic burner show the highest exergy destruction between the other compartments of the hybrid system and, hence, leave room for improvements.

Acknowledgements

The authors acknowledge the support provided by Enbridge Inc., the Natural Science and Engineering Council of Canada and the Ontario Research Fund through the Ontario Fuel Cell research and Innovation Network.

References

[1] R. Singh, Chemical Engineering Progress (1999) 59–66.
[2] G.H.J. Broers, J.A.A. Ketelaar, High temperature fuel cells, Industrial and Engineering Chemistry (52) (1960) 303–306.
[3] G. De Simon, F. Parodi, M. Fermeglia, R. Taccani, Journal of Power Sources (115) (2003) 210–218.
[4] H. Maru, H. Ghezel-Ayagh, A.J. Leo, Abstracts of the VII Grove Fuel Cell Symposium, London, 2001, pp. 797–800.
[5] E. Liese, R.S. Gemmen, Proceedings of the ASME Turbo Expo 2002, Amsterdam, 2002, pp. 341–349.
[6] M. Gnann, Abstracts of the VII Grove Fuel Cell Symposium, London, 2001.
[7] S.H. Chan, C.F. Low, O.L. Ding, Journal of Power Sources (103) (2002) 188–200.
[8] M.W. Chase, NIST-JANAF Thermochemical Tables, forth ed., Journal of Physical Chemistry Reference Data, Monograph 9 (1998) 1–1952.
[9] Exergoecology Portal Web page, http://www.exergoecology.com.
[10] D. Poulikakos, S.M. Senn, N. Hotz, Journal of Power Sources (158) (2006) 333–347.
[11] J.H. Koh, B.S. Kang, H.Ch. Lim, AIChE Journal 47 (9) (2001) 1941–1956.
[12] I. Dincer, Energy Policy (30) (2002) 137–149.
[13] J. Szargut, D.R. Morris, F.R. Steward, Exergy Analysis of Thermal, Chemical and Metallurgical Processes, Hemisphere, New York, 1988.
[14] M.A. Rosen, The development and application of a process analysis methodology and code based on exergy, cost, energy and mass', Ph.D. thesis, University of Toronto, Toronto, Canada, 1986.